Title

New approach to investigate the cytotoxicity of nanomaterials using single cell mechanics.

Journal

The journal of physical chemistry. B, 118(5)

ISSN

1520-6106

Authors

Zimmer, Christopher C
Liu, Ying X
Morgan, Joshua T
et al.

Publication Date

2014-02-01

DOI

10.1021/jp410764f

Peer reviewed

THE JOURNAL OF PHYSICAL CHEMISTRY B

Article

pubs.acs.org/JPCB

New Approach to Investigate the Cytotoxicity of Nanomaterials Using Single Cell Mechanics

Christopher C. Zimmer,[†] Ying X. Liu,[†] Joshua T. Morgan,[‡] Guohua Yang,[†] Kang-Hsin Wang,[†] Ian M. Kennedy,[‡] Abdul I. Barakat,[‡,§] and Gang-yu Liu*,[†]

[†]Department of Chemistry, University of California, Davis, One Shields Avenue, Davis, California 95616, United States

[‡]Department of Mechanical and Aeronautical Engineering, University of California, Davis, One Shields Avenue, Davis, California 95616, United States

[§]Hydrodynamics Laboratory (LadHyX), CNRS UMR7646, Ecole Polytechnique, 91128 Palaiseau, France

ABSTRACT: Current in vitro methods to assess nanomaterial cytotoxicity involve various assays to monitor specific cellular dysfunction, such as metabolic imbalance or inflammation. Although high throughput, fast, and animal-free, these in vitro methods suffer from unreliability and lack of relevance to in vivo situations. New approaches, especially with the potential to reliably relate to in vivo studies directly, are in critical need. This work introduces a new approach, single cell mechanics, derived from atomic force microscopy-based single cell compression. The single cell based approach is intrinsically advantageous in terms of being able to directly correlate to in vivo investigations. Its reliability and potential to measure cytotoxicity is evaluated using known systems: zinc oxide (ZnO) and silicon dioxide (SiO_2) nanoparticles (NP) on human aortic endothelial cells (HAECs). This investigation clearly indicates the reliability of single cell compression. For example, ZnO NPs cause significant changes in force vs relative deformation profiles, whereas SiO_2 NPs do not. New insights into NPs−cell interactions pertaining to cytotoxicity are also revealed from this single cell mechanics approach, in addition to a qualitative cytotoxicity conclusion. The advantages and disadvantages of this approach are also compared with conventional cytotoxicity assays.

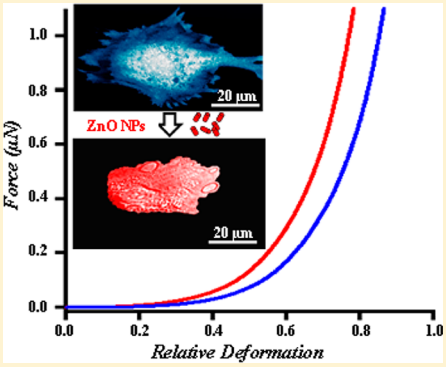

INTRODUCTION

Engineered nanomaterials have sparked an increasing demand for high throughput production, structure characterization, and toxicity assessments because of their potential applications in material science, devices, and biomedicine.[1−4] The small size (<100 nm) of nanoparticles (NPs) could lead to broad biodistributions in vivo.[5] In addition, the physiochemical properties of these NPs can lead to cytotoxicity in vivo.[3,6−9] Further, industrial quantities of nanomaterials have raised concerns about the potential acute and chronic health and environmental impacts following their release.[10,11]

Two primary approaches have been employed to assess nanotoxicity: in vivo toxicity studies using either animal models or data collected from human subjects[8,12−19] and in vitro methods such as cytotoxicity assays.[6,20−23] The former has advantages of reliability and more direct physiological relevance but suffers from various limitations including low speed, high complexity, high cost, and issues involving animal and human subjects.[4,8,12] The latter is high throughput, simple, and animal-free but faces challenges regarding in vivo relevance and reliability.[8,20−25] In contrast to the toxicity of small molecular drugs and chemicals, direct correlation of in vitro assays and in vivo toxicity for nanomaterials is very difficult because of the intrinsic and unique complexity of nanomaterials including (a) structural and functional changes of NPs during in vivo transport differing from in vitro exposure,[22,26] (b) possible reactions between nanomaterials and assay agents,[24,27,28] (c) the unrealistically high doses of nanomaterials that are necessary for in vitro assays,[24,29] and (d) lack of in vivo relevance of monoculture systems.[7] There is a critical need for new approaches and investigations that ultimately allow the correlation of in vitro with in vivo toxicity studies. One approach to address this challenge is to provide better in vitro mimetics to improve in vivo relevance, such as using coculture cells[30] or complex organ models.[31] Another approach is to provide better readout at the cellular level (i.e., regardless of the history of the NPs−cell interactions, measurements shall focus on the final outcome of the cells). This is analogous to the "equivalent circuit" approach. The present work reports a new means to read the behavior at a single cell level.

This article introduces a new physical chemistry technique, atomic force microscopy-based single cell compression, and the preliminary investigation regarding its potential to fulfill such a need for nanotoxicity assessment in vitro. This method shows great sensitivity to overall cellular behavior, including cell type, viability, membrane integrity, and cytoskeleton changes.[32−36] In principle, single cell mechanics is a good candidate to fulfill the need, because it is based on individual cells and, as such, can

Received: October 31, 2013
Revised: January 8, 2014
Published: January 13, 2014

   dx.doi.org/10.1021/jp410764f | J. Phys. Chem. B 2014, 118, 1246−1255

directly probe cellular behavior from cells in vitro and in vivo. Therefore, it should be capable of bridging in vitro with in vivo studies by reading single cell mechanics. Additionally, because cell mechanics is a result of overall cellular behaviors, this method enables probing the collective well-being of cells instead of a single dysfunction, such as metabolic dysfunction read by MTT assays.[7,25]

Using known cytotoxicity studies, this work evaluates the reliability and sensitivity of this method by performing treatment under the same conditions and testing the outcomes. In addition, this investigation also demonstrates that this new approach could provide new insights into NPs−cell interactions. Human aortic endothelial cells (HAECs) were used in this study because they are known to uptake metal oxide NPs in a dose dependent manner in vitro.[37] Because inhaled aerosolized NPs can cross the pulmonary epithelial barrier into the bloodstream, exposing vascular endothelial cells which would exhibit a dose dependent affinity to NP uptake,[38,39] HAECs provide a good cell model system for evaluating efficacy of cytotoxicity studies as its cytotoxicity is well studied by us and others.[37,40−44] Selected NPs include zinc oxide (ZnO) and silicon dioxide (SiO_2). ZnO NPs were found to be cytotoxic according to bioassays.[37,45−47] Inflammation appeared to be a primary consequence as mRNA and protein inflammatory markers were increased upon treatment.[37] In contrast, under the same treatment conditions as ZnO, SiO_2 NPs did not induce inflammation under similar conditions nor did they exhibit significant cytotoxicity;[48,49] SiO_2 NPs only exhibit toxicity through loss of cell viability,[2] ROS production,[48−50] mitochondrial dysfunction,[48] and membrane disruption[49] at much higher dosage and longer duration exposure.

EXPERIMENTAL METHODS

Synthesis and Characterization of Oxide Nanoparticles. ZnO NPs were synthesized following protocols described previously.[37] A Zn shot (99.999%; Alfa Aesar, Ward Hill, MA) was placed in a stainless steel furnace that was heated to approximately 600 °C. Metallic Zn vapor was seeded into an H_2/air diffusion flame.[51] The postflame aerosol containing the particles was drawn into a sampling tube by vacuum and the particles were captured on a filter.

SiO_2 NPs with a tetramethylrhodamine-5(6) isothiocyanate (TRITC) core (enabling fluorescence imaging) were synthesized via a microemulsion method incorporating the dye covalently bound to the silica matrix. Reagents were purchased from Sigma-Aldrich Corp. (St. Louis, MO). TRITC was conjugated to the silica precursor aminopropyltriethoxysilane (APTS) in an anhydrous environment using an excessive amount of APTS for 24 h. Then, the microemulsion system was formed by mixing cyclohexane (oil), Triton X-100 (surfactant), *n*-hexanol (cosurfactant) (4.2/1/1, V/V/V) and an appropriate amount of water under stirring. Tetraethylorthosilicate (TEOS) and the TRITC-APTS precursor were added after the addition of ammonia (volume ratio of TEOS to ammonia was 1.7) into the mixture. The reaction proceeded over a period of 24 h at room temperature. The NPs were isolated from the microemulsion using ethanol, centrifuged, and washed with ethanol and water several times.

NPs were characterized using transmission electron microscopy (TEM), X-ray diffraction (XRD), and the Brunauer−Emmett−Teller (BET) methods.[37] ZnO NPs used in this investigation were rod-shaped with lengths of 100−200 nm and diameters of 20−70 nm.[37] SiO_2 NPs were spherical with diameters of 96 ± 15 nm. NP stock solutions were prepared by adding dry NPs to distilled water to concentrations of 2 and 3.3 mg/mL for ZnO and SiO_2 NPs, respectively. The stock solutions were sonicated for 5 min to break up aggregates and diluted using antibiotic free Endothelial Growth Media-2 (EGM-2, Lonza, Basel, Switzerland) to the designed concentrations (e.g., 10 and 50 μg/mL) prior to cell treatments. Henceforth, dosages of 10 and 50 μg/mL are referred to as the low and high dosage, respectively.

Cell Culture and Treatment. Type 1 rat tail collagen was diluted to 100 μg/mL in 0.02 M acetic acid (BD Biosciences, San Diego, CA) and applied to Mat-Tek glass bottom dishes (MatTek, Ashland, MA) for 30 min at 37 °C. HAECs (Cascade Biologics, Portland, OR) in passages 5−6 were then plated at subconfluent density. The cells were maintained in EGM-2 media and incubated overnight (37 °C, 5% CO_2). Upon washing with fresh EGM-2 solution, cells were incubated with 1.5 mL of the NP solutions described in the previous section for 4 h and then immediately placed on the AFM stage for the designed cell mechanics investigations.

Isolation of RNA and Reverse Transcription. Immediately following incubation with ZnO NPs, cell culture supernatants were collected and stored at −20 °C for future enzyme-linked immunosorbent assay (ELISA) of soluble intracellular cell adhesion molecule-1 (ICAM-1). The cells were subjected to total RNA purification using an RNeasy mini kit (Qiagen, Valencia, CA) according to manufacturer's protocol. cDNAs were prepared from 1 μg total RNA using the reverse transcriptase iScript cDNA Synthesis kit (Biorad, Hercules, CA) according to the manufacturer's instructions.

Quantitative Real-Time Polymerase Chain Reaction Analysis. Transcription levels of three inflammatory markers, intercellular adhesion molecule 1 (ICAM-1), monocyte chemotactic protein-1 (MCP-1), and interleukin-8 (IL-8), were measured by real-time PCR. Gene-specific probes and primer mix were purchased from Applied Biosystems, Grand Island, NY (ABI TaqMan gene expression assay).

Quantitative real-time PCR was conducted using a 7900 HT Fast Real-time PCR system (Applied Biosystems, Grand Island, NY). The reaction was performed in 96-well Optical Reaction Plates (Applied Biosystems, Grand Island, NY) with 10 μL of reaction mixture in each well. The reaction mixture contained samples of cDNA diluted at 1:2, probe and primer mixed, and Faststar Universal probe Master (ROX) purchased from Roche (Indianapolis, IN). Expression levels of inflammatory genes were normalized to GAPDH for each sample. Treatment with 1 μg/mL of lipopolysaccharide (LPS) served as a positive control.

Single Cell Compression. Single cell compression was developed by our team and described previously.[35] As depicted in Figure 1, a cell is compressed between the spherical probe and glass substrate. Briefly, probes were modified silicon cantilevers (AC240, Asylum Research, Santa Barbara, CA) with glass sphere of a diameter of 60 ± 4 μm (Duke Scientific, Fremont, CA) attached to the tips, using a premixed two-component epoxy (S-31, ITW Performance Polymers, Riviera Beach, FL). After sphere attachment, the spring constant was calculated as 1.58 N/m based on the added mass method[52] and sphere placement correction method.[53]

Probe-microsphere position was guided, with regard to the target cell, by an IX50 inverted optical microscope (Olympus America, Center Valley, PA) integrated in-house onto an AFM scanner (MFP-3D, Asylum Research, Santa Barbara, CA). A CCD camera was used to monitor and record cellular

dx.doi.org/10.1021/jp410764f | J. Phys. Chem. B 2014, 118, 1246−1255

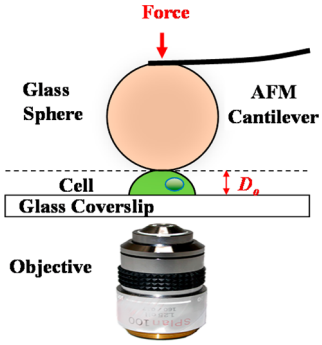

Figure 1. Schematic diagram illustrating the concept of the single cell compression methodology.

morphology during the compression cycle. In this investigation, the center of the probe was positioned above the highest point at the edge of the nucleus in order to minimize nuclear contribution.

In the case of SiO_2 treatment, the cells were imaged on a Nikon TE300 Eclipse inverted microscope (Nikon Inc., Melville, NY) with a 40X Plan Fluor objective (NA = 0.6). A Retiga 1300 monochrome camera (Q-Imaging, Surrey, British Columbia, Canada) coupled with QCapture Imaging Suite was used to confirm visible TRITC illumination from the SiO_2 NPs and cell loading.

Force−deformation profiles were first acquired on the bare substrate nearby to establish an internal reference and force profile for calculating cell height. The compression was performed at a relatively low rate of 2 μm/s to minimize hydrodynamic contributions and to enable extraction of elastic compliance.[35] All cell compression experiments were completed within 30 min starting with removal from the incubator to ensure viability of the cells. Individual cell viability was also confirmed using trypan blue stain (21 μM, Invitrogen, Carlsbad, CA) as described previously.[35] For each experiment, 2−4 sets of measurements were taken. In each set, 3−8 characteristic cells were chosen under optical objective for mechanical measurement.

For cells without major geometric changes due to NP treatments, the profiles are displayed as force vs relative deformation (ε);[35] those with severely altered morphology are represented in force vs relative volume displacement (RVD) plots as detailed in previous work.[36] Relative deformation, ε, is defined as change in height (Δz) over the initial cell height (D_0). RVD is defined as displaced volume over the initial cell volume. The initial volume is estimated from microscopy measurement using the ellipsoid cap approximation.[36] Cell volume was calculated using lateral measurements taken from optical images of the cells on the substrate and from initial cell height measured by AFM. The cell shape was modeled as an ellipsoid cap, which was shown to be a good approximation by AFM imaging. The procedure and formula for calculating the volume of an ellipsoid cap were reported previously.[36]

Results are presented as mean ± standard deviation (SD). Statistical analysis was performed by an unpaired, two-tailed Student's t-test. Differences in means were considered significant if $p < 0.05$. For the ε values of ZnO 10 in Table I, for example, the t test performed at F = 50 and 300 nN, resulted in t = 3.5 and 4.2, with p value of 0.0008 and <0.0001, respectively, showing there is no similarity among the treated and control cells. For the E_m values of ZnO 10 and ZnO 50 (a) shown in Table II, t = 2.5 and 6.2, respectively, again confirming the stiffening effect is statistically significant (>99.9%). The data with significant differences (p value <0.05) from the control are indicated using bold font in Tables I and II.

RESULTS

Inflammation and Viability upon Treatment with ZnO NPs. Prior in vitro work suggests that 10 and 50 μg/mL ZnO NP treatment induces cellular inflammation, as well as a reduction in membrane integrity[54] and mitochondrial activity.[51,54,55] An inflammatory pathway appears to be the dominant response at the early stage following NP treatment while the cells are still living.[37] Therefore, we compare our measurements with in vitro inflammation assays. Prior studies also suggest that in vitro cytotoxicity assay results are sensitive to the history of cells and NPs.[46] In order to make a meaningful comparison for this investigation and test the sensitivity of our technique, cytotoxicity assays were carried out in parallel with single cell compression experiments following identical treatment conditions. Incubating HAECs for 4 h with 10 μg/mL of ZnO NPs induced 1.4 ± 0.5 and 1.5 ± 0.2 fold increases in ICAM-1 and IL-8 mRNA levels relative to control, whereas MCP-1 mRNA levels remained unchanged, as shown in Figure 2. At 50 μg/mL, all inflammation markers, ICAM-1, IL-8, and MCP-1 mRNA levels increased, especially ICAM-1 at 4.4 ± 0.2 fold in comparison to control ($p < 0.05$), suggesting a dose-dependent increase in cell inflammation. The ICAM-1 level induced by the high dosage ZnO NP treatment were approximately 25% of those induced by the positive control treatment (1 μg/mL lipopolysaccharide (LPS) for 4 h). The change in the other inflammation markers, namely IL-8 and MCP-1, was small relative to ICAM-1, possibly suggesting that the inflammation pathways differ from LPS-triggered processes.

At 10 μg/mL ZnO NPs treatment, cell loss was below 20% after 4 h, whereas at 50 μg/mL, there was a 50% loss of cell

Table I. Comparison of Geometry and Mechanical Properties of HAECs before and after Exposure to Designated Nanoparticles

cell and NPs	control	ZnO 10	ZnO 50 (a)	ZnO 50 (b)	SiO_2 10	SiO_2 50
[NP] (μg/mL)	0	10	50	50	10	50
cell height (μm)	4.4 ± 0.7	6.2 ± 1.9	6.6 ± 1.6	12.4 ± 3.8	4.4 ± 0.4	5.0 ± 0.4
volume (μm^3)	1700 ± 500	3600 ± 1800	4800 ± 1700	7500 ± 2200	1800 ± 400	2700 ± 700
Δz (μm) @ F = 50 nN	2.0 ± 0.4	2.2 ± 0.5	2.0 ± 0.8	4.5 ± 1.3	1.8 ± 0.2	2.4 ± 0.4
ε @ F = 50 nN	0.45 ± 0.05	**0.36 ± 0.04**	**0.30 ± 0.09**	**0.36 ± 0.04**	0.42 ± 0.06	0.48 ± 0.03
RVD @ F = 50 nN	0.11 ± 0.02	0.07 ± 0.01	0.04 ± 0.02	0.08 ± 0.02	0.09 ± 0.02	0.11 ± 0.01
Δz (μm) @ F = 300 nN	3.1 ± 0.5	3.5 ± 0.7	3.4 ± 1.3	7.9 ± 2.7	3.0 ± 0.3	3.7 ± 0.4
ε @ F = 300 nN	0.71 ± 0.06	**0.58 ± 0.06**	**0.51 ± 0.10**	**0.63 ± 0.03**	0.68 ± 0.04	0.74 ± 0.02
RVD @ F = 300 nN	0.27 ± 0.04	0.17 ± 0.02	0.12 ± 0.05	0.32 ± 0.04	0.24 ± 0.02	0.26 ± 0.01

dx.doi.org/10.1021/jp410764f | J. Phys. Chem. B 2014, 118, 1246−1255

Table II. Comparison of Membrane Young's Modulus and Ion Flux Dysfunction of HAECs Treated with Various Oxide Nanoparticles

cell and NPs	[NP] (μg/mL)	E_m(MPa)	ΔF (nN) @ RVD = 0.2	ΔC (μM) @ RVD = 0.2	[Zn^{2+}] (μM) if fully dissolved
control	0	5.0 ± 2.1	0	0	0
ZnO 10	10	**7.7 ± 1.8**	**273 ± 166**	**153 ± 79**	123
ZnO 50 (a)	50	**16 ± 12**	**446 ± 218**	**175 ± 88**	614
ZnO 50 (b)	50	3.8 ± 1.7	−34 ± 33	−14 ± 22	614
SiO_2 10	10	5.5 ± 0.8	28 ± 40	20 ± 8	N/A
SiO_2 50	50	3.7 ± 1.5	−1 ± 16	−41 ± 29	N/A

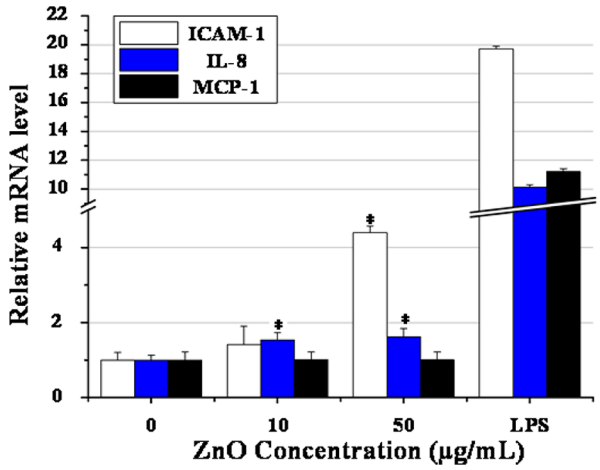

Figure 2. Relative mRNA levels of the three inflammatory markers ICAM-1, IL-8, and MCP-1 for HAECs incubated with ZnO NPs for 4 h at various concentrations. Treatment with 1 μg/mL LPS served as a positive control. Each mRNA value was normalized to corresponding GAPDH value. Relative mRNA levels are calculated as fold ratios relative to control cells. Measurements are mean ± SD from experiments run in triplicate.

viability, as measured by the trypan blue exclusion assay. In contrast, under the same treatment conditions, SiO_2 NPs had little effect on HAEC viability (>90% viable).

ZnO NPs at Low Dosage Led to Cellular Stiffening. A typical HAEC force-deformation profile is shown in Figure 3

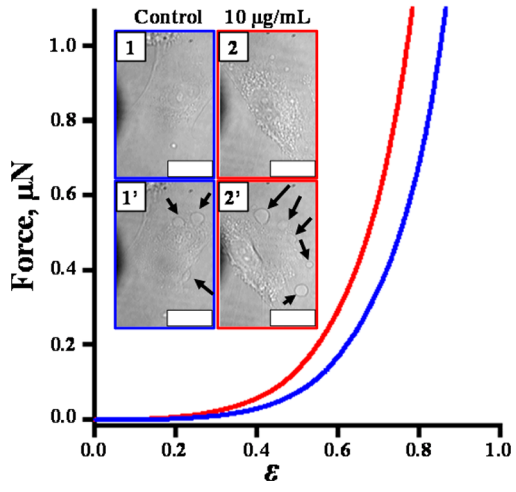

Figure 3. Typical F vs ε profiles for control (solid blue) and for treatment with 10 μg/mL ZnO NPs (solid red). The inset shows bright field optical images of the HAECs taken before (top) and immediately after (bottom) compression. Black arrows point to the blebs observed due to compression. Scale bar = 20 μm.

(blue). During cell compression, force−deformation profiles are acquired in both loading and unloading cycles. Although cell-probe adhesion could be extracted from the unloading, this region of the profiles is omitted to focus on cellular mechanics instead of adhesion. The F vs ε profiles appear smooth (without stress peaks) and nonlinear, similar to those of fibroblast cells.[36] Trypan blue assay results demonstrated that untreated HAECs could survive up to three sequential compressions with loads >1 μN with 2−3 min recovery time. As a comparison, Jurkat T lymphocyte cells survived less than a full compression cycle, during which membranes ruptured,[35] manifesting as stress peaks. The resilience of HAEC membrane is, thus, higher than that of T cells[35] but lower than that of neuronal cells, which sustain 4 cycles.[34] The mechanical strength falls between neuronal cells (N2a) and keratinocyte cells.[33,34] The optical micrograph in Figure 3 shows a typical (>99% population) morphology of a living control HAEC before (inset 1) and after (inset 1′) compression. Cells exhibit an ellipsoidal shape at the soma with broad and relatively flat lamellae around the periphery. From tens of cells in nine sets of experiments, the long and short semiaxes measured 22 ± 4 μm and 11 ± 2 μm, respectively, with a height of 4.4 ± 0.7 μm (Table I). The shape and size corresponded well with known dimensions of healthy endothelial cells.[56,57]

Adding 10 μg/mL ZnO NPs to cell culture media led to cell height and volume increases of 48% and 112%, respectively, for the example cell shown in Figure 3. Under an optical microscope, the contrast appears clearer and more heterogeneous (Figure 3, inset 2). Control cells generally developed multiple blebs at high deformation (>50%), as indicated in Figure 3 (inset, 1′, 3 blebs). Upon unloading, blebs retracted and took 2−3 min to vanish. Higher degrees of blebbing were observed for ZnO NP treated cells, as shown in Figure 3 (inset 2′, 5 blebs). This observation could be rationalized by intercalation of ZnO NP within the cell membrane[37] and cytoskeleton, which manifests into higher membrane heterogeneity and enhancement in optical contrast.

Because most HAECs retain their shape despite swelling, F vs ε profiles provide a reliable comparison, as shown in Figure 3. The profile of treated cells appears left-shifted with respect to the control, indicating stiffening during the entire compression process. At a low load of 50 nN, for example, a cell was compressed by 38% and 45% of its original height for treated and control cells, respectively. At a higher load of 300 nN, treated cells continue to deform less (60%) in comparison to the controls (71%). The results are consistent among all 25 measurements from four separate experiments, as summarized in Table I.

Although the cytokine assay (Figure 2) only detected mild inflammation at this dosage, F vs ε profiles showed clear and significant differences in terms of mechanics in both membrane and cytoskeleton.

dx.doi.org/10.1021/jp410764f | J. Phys. Chem. B 2014, 118, 1246−1255

ZnO NPs at Higher Dosage Led to Significant Changes in Cell Morphology and Mechanics. Under the same treatment time of 4 h, a 50 μg/mL ZnO NP dosage resulted in dramatic changes in cellular morphology. Under optical microscopy, two representative populations could be observed: (a) 30% of the cells exhibited a shape similar to cells shown in Figure 3 inset 2 but were much more swollen; and (b) 70% of the cells revealed retracted and round boundaries with a much higher degree of swelling. An additional 1 h of exposure time to the NPs (5 h total) led to an almost 100% population with retracted and round boundaries with a much higher degree of swelling, as in category b. Further incubation (6 h total) resulted in 100% cell death. This time-dependent swelling and cell death suggest the possibility of significant ion flux dysfunction.

A representative cell (Figure 4A) from the first subpopulation was 7.9 μm tall with a volume of 4775 μm^3. Because cell geometry varies after treatment, a meaningful comparison in cell mechanics is made using F vs RVD profiles.[36] The treated cell profile in Figure 4C (red) is a typical force profile of these cells, which is significantly left-shifted from the control, indicating stiffening through all of the deformation range. At both 50 and 300 nN loads, for instance, this cell deformed by 66% and 53% less, respectively, in comparison with that of the control. Results from four experiments revealed consistent outcomes (Table I).

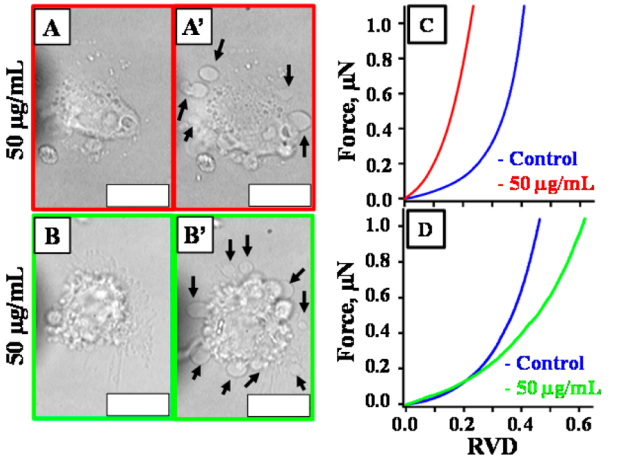

Figure 4. Bright field optical images taken before (left) and immediately after (right) compression of minority and majority populations of HAECs treated with 50 μg/mL ZnO NPs. Black arrows point to blebs formed during compression. Scale bar = 20 μm. F vs RVD profiles for three representative cells are shown in (C) and (D): control (blue), for minority (red), and majority populations (green), respectively.

The second subpopulation exhibited significant swelling; that is, the cell in Figure 4B showed height and volume increases of 1.45 and 3.30-fold, respectively. In the F vs RVD profiles, the second population overlaps with the control at low deformation (RVD < 25%) but is right-shifted at higher deformation (RVD > 25%) (Figure 4D), indicating softening. These observations differ significantly from those of Figure 3 and in Figure 4C, especially the fact that the cytoskeletons become much softer with dosage and time. For instance, at 300 nN, these cells deform 22% more than do the control, in terms of RVD. Among tens of cells from four experiments, this trend remained qualitatively and quantitatively valid (Table I).

A higher degree of blebbing was observed for population b. For example, five blebs were observed in Figure 4A′, and nine blebs were observed in Figure 4B′. Upon unloading, blebs remained for the duration of the measurements, in contrast to control and low dosage treatments. These observations can be rationalized by more ZnO uptake by membrane and intracellular components, leading to heterogeneity of cellular membrane (more blebbing), ion flux dysfunction (swelling), and weakening of the cytoskeleton (soft profile).

Figure 2 shows an increase in ICAM-1 at 50 μg/mL, indicating a higher degree of inflammation than ICAM-1 at 10 μg/mL. The changes in single cell mechanics not only reflect the occurrence and severity of inflammation but also suggest mechanistic information: uptake of ZnO NPs by membrane and intracellular components leads to increased blebbing, ion flux dysfunction (swelling), and permanent damage of the cytoskeleton, which eventually leads to cell death. This new single cell compression based approach probes overall cellular dysfunction and provides a reliable, sensitive, label-free, and quantitative method to assess nanotoxicity in vitro.

Treatments with SiO_2 NPs Led to Little Change in Cellular Mechanics. Treating HAECs with 10 μg/mL SiO_2 NPs for 4 h did not lead to observable changes in cell height and volume (Table I). A typically treated cell in Figure 5B shows only minute enhancement and heterogeneity in optical contrast. Upon loading, blebbing behavior was also similar to that of the controls (Figure 5B′, 1 bleb, and Figure 5A, 0 blebs), indicating that membrane heterogeneity remained similar to the control upon treatment. Using TRITC labeled SiO_2 NPs in a parallel experiment, emission at 557 nm was clearly visible under epifluorescence microscopy, thus confirming NP uptake (data not shown).

With little change in geometry, F vs ε profiles provide reliable comparison of cellular mechanics,[34,35] as shown in Figure 5D. The profiles of treated cells exhibited almost identical behaviors as control profiles. At 50 nN and 300 nN load, this treated cell is compressed by 42% and 71% of its original height, respectively, which is almost identical to the control. These values and the trend were reproducible (Table I). The lack of detectable changes in cell mechanics is consistent with prior knowledge that higher SiO_2 NP concentrations or longer treatment times are required to elicit a biological response in endothelial and other cell types.[2,48,50]

Cells undergoing a 50 μg/mL SiO_2 NP treatment exhibited higher degrees of optical heterogeneity, although their morphologies resembled control cell morphologies. A typical treated cell is shown in Figure 5C. Upon loading, treated cells exhibit similar blebbing behavior as the control cells. The small degree of swelling is quantified in Table I. The highly overlapping F vs ε profile of a typical treated cell and control indicates SiO_2 NP treatment, even at high dosage, does not induce appreciable mechanical change (Figure 5E). At a relatively low force of 50 nN and a relatively high force of 300 nN, the treated cells deform by 43% and 72%, respectively, which are almost identical to deformations of control cells. The trend and values are consistent for all cells in three separate experiments.

Quantification of Young's Modulus of Cellular Membrane. To quantify membrane Young's moduli (E_m) from F vs ε profiles, we adopt Hertzian contact mechanics and assume that the cells behave like balloons filled with incompressible fluid.[35] When a balloon is compressed between

dx.doi.org/10.1021/jp410764f | J. Phys. Chem. B 2014, 118, 1246−1255

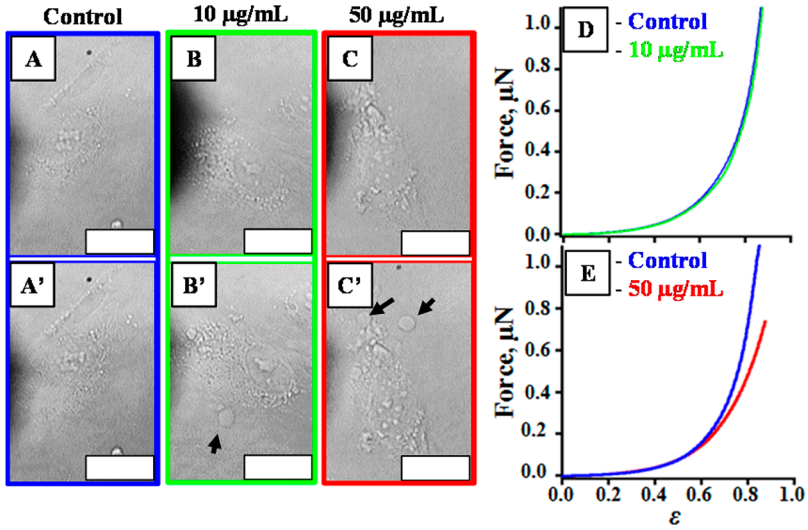

Figure 5. Bright field optical images taken before (top) and immediately after (bottom) compression of control, cells treated with 10 μg/mL, and 50 μg/mL SiO_2 NPs for 4 h. Black arrows point to blebs formed due to compression. Scale bar = 20 μm. Typical F vs ε profiles for three representative cells are shown in (D) and (E): control (blue), 10 μg/mL (green), and 50 μg/mL (red) SiO_2 NP treated HAECs.

two parallel plates (Figure 6A), the F vs ε profile follows a cubic power law as expressed in eq 1

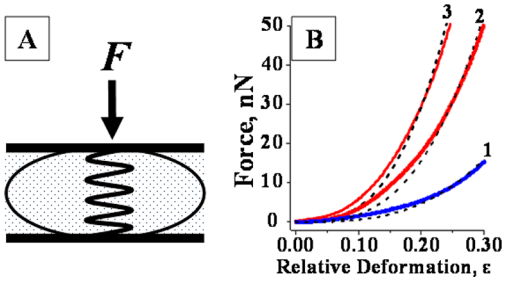

Figure 6. (A) Schematic of the balloon model, in which external force causes the membrane to stretch and bend. The membrane mechanical signature can be quantified by Young's modulus and bending constant. (B) F vs ε profiles at low deformation region of a control (blue, 1), 10 μg/mL ZnO NP treated (red, 2), and the minority population of the 50 μg/mL ZnO NP treated (red, 3) HAECs. The results from least-squares fitting using eq 1 are plotted in dashed lines, which indicate excellent agreement with the force profiles.

$$F_m = 2\pi \frac{E_m}{1-\nu_m} h R_0 \varepsilon^3 \quad (1)$$

where ε represents relative height changes and ν_m is the Poisson ratio of the cell (ν_m = 0.5, assuming HAECs are perfectly incompressible). R_0 and h are the initial cell radius (half of the cell height) and cell membrane thickness (we assume h = 4 nm), respectively. Using eq 1 and a measured F vs ε profile, least-squares fitting would yield E_m, as summarized in Table II. This model has been shown to be effective at small deformations (<30%), where the membrane remains impermeable and intracellular contributions (by the cytoskeleton, for example) are relatively small.[58−60]

Figure 6B illustrates the measured (solid) and least-squares fitted (dashed lines) profiles at ε = 0−30% for control (blue, 1), treatment with 10 μg/mL (red, 2), and treatment with 50 μg/mL ZnO NPs [population (a), red, and 3], respectively. The typical HAEC (blue, 1) shows a very good agreement between fitting and measurements, and the membrane E_m = 5.0 MPa with $\chi^2 = 4 \times 10^{-16}$. At dosages of 10 and 50 μg/mL, the HAECs membrane Young's modulus increases to 9.0 and 13.0 MPa with $\chi^2 = 4.1 \times 10^{-15}$ and 2×10^{-14}, respectively. This trend is consistent for all experiments, as summarized in Table II. The increase in E_m can be rationalized by ZnO NPs embedded within the membrane, thereby reducing the fluidity. The increased blebbing and membrane heterogeneity provide further support for this conclusion. The increase in E_m at high dosage indicates more ZnO NPs are within membrane. For population (b) at 50 μg/mL, E_m decreased to 4.4 MPa accompanied by severe swelling and softening of the cytoskeleton. This can be rationalized by more intracellular NPs and dissolution of ZnO NPs, which could lead to ion flux dysfunction and cytoskeletal damage. This conclusion is consistent with previous studies, which found ZnO NPs within the membrane[37] and in the cytoplasm near the cell membrane and nucleus[61] as well as in endocytotic vesicles.[37,41,61] Further, this method could provide quantitative measurement of NP uptake at cellular membrane and cytoskeleton upon systematic calibration.

In the case of SiO_2 treatment, the membrane Young's modulus is almost identical to that of the control (Table II). Considering also the similarity in blebbing behaviors and the lack of severe swelling, as well as the uptake of NPs, we infer that SiO_2 NPs are likely to distribute homogeneously within the cell with only benign effects.

Single Cell Compression Measurements Enable Estimation of Ion Flux Dysfunction. Given the severe swelling and uptake of ZnO NPs, ion flux dysfunction is expected to have occurred.[34] Assuming the observed left shift in F vs ε profiles is solely due to ion flux dysfunction, we could estimate the ion concentration change following established methods.[34]

The increase in osmotic pressure could be estimated using the F vs ε profiles,[34] or from F vs RVD profiles, following eq 2

$$\Delta F = \Pi \cdot S \quad (2)$$

where ΔF, Π, and S are excess force, increase in osmotic pressure, and cell-probe contact area, respectively.

The contact area, S, between the glass bead and the ellipsoid cap-shaped cell can be calculated using eq 3

dx.doi.org/10.1021/jp410764f | J. Phys. Chem. B 2014, 118, 1246−1255

$$S_{(\mathrm{RVD})} = \pi \sqrt{a^2\left(1 - \frac{(c-z)^2}{c^2}\right)} \sqrt{b^2\left(1 - \frac{(c-z)^2}{c^2}\right)} \quad (3)$$

where a, b, and c are the three major semiaxes defining the ellipsoid and z is the distance from the glass substrate to the center of the glass sphere or probe, which depends upon the value of RVD.[36] The values for a, b, and c were generated from simultaneous fitting[36] using optical microscopy measurement and AFM height measurement; ΔF is extracted from the two F vs RVD profiles, and $\prod$ can then be calculated from eq 2.

Uptake of ZnO NPs into cells could impact cellular membrane by creating membrane discontinuities[37] and increase plasma membrane permeability.[54,62,63] The molar concentration increase, ΔC, can be calculated from the osmotic pressure-ion concentration relation,[34] using eq 4

$$\Delta C = \frac{\Pi}{RT} \quad (4)$$

where R is the gas constant, and T is the experiment temperature (298 K). At RVD = 0.2, the ΔC for each treatment is summarized in Table II. At 4 h exposure to 10 μg/mL ZnO NPs, ΔC is 153 ± 79 μM. Assuming all NPs taken up were completely dissolved, $[Zn^{2+}]$ = 123 μM. The ΔC value is slightly larger than the maximum $[Zn^{2+}]$, which indicates that osmotic pressure is primarily responsible for the observed F vs ε and F vs RVD shifts at low deformation. At 50 μg/mL dosage, ΔC = 175 ± 88 μM, for cells without dramatic morphological changes. This minute increase in comparison to 10 μg/mL treatment indicates that ionic dysfunction was maximized at the dosage of 10 μg/mL. This indicates that ion flux dysfunction represents only one aspect of the ZnO NP toxicity response. Other indicators, as evidenced by changes in membrane and cytoskeleton integrity (previous section), become much more severe in 50 μg/mL treatment compared with that of 10 μg/mL. Further uptake most likely led to the higher number of ZnO NPs in membrane and intracellularly but exhibited no further impact of ion flux dysfunction for this subpopulation. For cells with dramatic change in morphology [population b], ΔC = −14 ± 22 μM, which means it is similar to the control. The fact that ion flux changed significantly then reverted back in conjunction with a dramatic change in cellular morphology and cytoskeleton is an indication of complete damage to membrane function (no longer serving as an osmotic membrane).

In contrast, uptake of SiO_2 NPs induced very little change in ion concentration in HAECs at the same dosage and time (Table II). This is consistent with the apparently benign nature of SiO_2.

Previous work indicates that internalized ZnO NPs could dissolve in cells due to the acidic environment (pH ∼ 5) within intracellular vacuoles, creating an osmotic pressure imbalance between the vacuole and the surrounding cytoplasm and causing vacuoles to undergo severe swelling.[10,37,41,45] Because of an NP's high surface-to-volume ratio, the dissolving process would be faster than bulk ZnO materials,[10,37,41,45] leading to an increase in overall ion concentration within our experimental time. Osmotic pressure would drive intracellular intake of water, causing swelling in vacuoles and the surrounding cytoplasm.[10,41,45] Our measurements of control, 10 μg/mL, and 50 μg/mL subpopulation a are consistent with the increase in overall ion concentration and swelling. In addition, our quantitative analysis using eq 1 and 4 provides new insights into the effects of ZnO NPs. At 10 μg/mL dosage, NPs enter cells and intercalate with the membrane, causing an increase in E_m. Intercalation of external entities into the membrane that result in a decrease in fluidity and an increase in E_m has been previously reported.[32,34] Intracellular NPs dissolve, causing an increase in ion concentration, swelling, and ion flux dysfunction. Increasing NP dosage leads to more NPs in cell membrane, as indicated by a higher E_m value but no further effect on ion flux dysfunction. With time, the failure of the ion pumps of the plasma membrane due to NP interference with ATP generation increases the permeability of the plasma membrane.[63] Eventually, the membrane fails, accompanied by cytoskeleton destruction and eventually cell death.

DISCUSSION

From the results reported above, the force profiles from the single cell mechanics study could provide a new assay for nanocytotoxicity. The validity of this approach has been demonstrated by reading force−deformation profiles following known NP treatments utilized previously. Clearly, the profile changes could indicate toxicity, such as the results at 10 μg/mL of ZnO NPs, which is known to cause inflammation as per in vitro assays.[37] The new insights revealed from this method are also encouraging. For example, although cytotoxicity assays yield only one number for each inflammatory marker over millions of cells, this new method enables readout of detailed outcomes. At 50 μg/mL ZnO NPs, for example, single cell mechanics measurements clearly revealed two types of cellular responses, with one more severely toxified than the other. Aside from confirming the degree of toxicity and dose-dependence of ZnO and SiO_2 NPs, the principle of cellular mechanics enables sensitive measurements of all foreign substances taken up by cells such as dyes and biochemicals.[32,34] In principle, this method only requires a single cell to yield informative measurements, thus exhibiting high sensitivity. The sensitivity and the enabled capture of diversity in responses are particularly relevant and advantageous in the context of correlation with in vivo studies, as in vivo cellular samples are difficult to harvest in massive and uniform populations and do present high individualities. This approach could enable individual samples from in vivo sources to be studied one by one to yield meaningful information regarding NP uptake and mechanical changes. One challenge in nanocytotoxicity is to examine repeated and time-dependent exposures reliably; our approach could address this challenge, as one batch of samples may be subjected to repeated exposure and time-dependent studies in situ under the same experimental setting to yield meaningful and reliable results. Finally, measurements of cell mechanics also provide quantitative information such as the Young's moduli of the membrane and cytoskeleton, as well as ion flux dysfunction, to shed new light on NPs−cell interactions.

As this approach is still in its infancy, we are also actively finding and addressing its limitations. For example, this method does not provide specific chemical information, such as markers, associated with cellular signaling cascades. We are exploring solutions by correlating with known cellular assays and implementing optical readout[64] in situ. This approach is also less routine compared with assay protocols. Only trained analytical chemists, engineers, and biophysical researchers are able to master this technique in a timely manner. Work is also in progress to make this method more user-friendly and "turn-key."

CONCLUSIONS

The work demonstrates that single cell mechanics provides a new and highly promising alternative to study the cytotoxicity of nanomaterials in vitro. Using previously known cytotoxicity of ZnO and SiO_2 NPs on HAECs, our study indicates that ZnO NPs exhibit dose-dependent changes in force-deformation profiles, whereas SiO_2 NPs show little impact under the same treatment conditions. The measured cellular mechanics are sensitive to dosage and treatment time. Therefore, the changes in F vs ε profiles provide a reliable and sensitive readout of NPs' cytotoxicity. In addition, from F vs ε and F vs RVD profiles, we have extracted the membrane mechanical property (E_m) and ion flux dysfunction (ΔC), respectively, which enables further understanding of NP−cell interactions and overall dysfunctions of cells. In comparison to conventional bioassays, this new approach is single-cell-based and, thus, could provide a direct linkage to in vivo studies. It is very sensitive and able to capture the response of individual cells, which is highly complementary to cytotoxicity assays, which usually only present a single output for a large population (>10^4) of cells. Further, single cell mechanics is label-free. There is need neither for lysis to extract cellular contents for assay nor for adding test reagents, eliminating false positives due to the biochemical reagents used in cellular assays. Finally, this method enables time-dependent study as well as direct comparison between in vitro and in vivo exposures, as getting single cells after exposure is much easier than alternative approaches. Little or no modification to the method is necessary for measuring single cell mechanics for cells harvested from a host for in vivo study. Given the key facts that this method is single-cell-based and cells from in vitro and in vivo means can be compared directly, this approach in principle could enable direct correlation between in vitro and in vivo measurements. Work is in progress to study time-dependent and dose-dependent nanotoxicity systematically, to compare single cell mechanics with other cellular responses such as metabolic dysfunction, and to establish equivalent exposure for in vitro and in vivo studies.

AUTHOR INFORMATION

Corresponding Author

*G.-y Liu. E-mail: gyliu@ucdavis.edu. Phone: 530 754-9678. Fax: 530 752-8995.

Notes

The authors declare no competing financial interest.

ACKNOWLEDGMENTS

We thank Drs. T. J. Mullen and A. Karsai for helpful discussions and Ms. S. Stagner for her assistance in the preparation of this manuscript. This work was supported by the W. M. Keck Foundation, University of California, Davis, a Cancer Research Coordinating Committee (CRCC) research grant, a permanent endowment in Cardiovascular Cellular Engineering (the AXA Research Fund), and the National Institute of Environmental Health Sciences (P42ES004699). Y.X.L. is a recipient of the GAANN Fellowship from the United States Department of Education (2009-2010).

REFERENCES

(1) Popov, A. P.; Lademann, J.; Priezzhev, A. V.; Myllyla, R. Effect of Size of Tio2 Nanoparticles Embedded Into Stratum Corneum on Ultraviolet-a and Ultraviolet-B Sun-Blocking Properties of the Skin. *J. Biomed. Opt.* **2005**, *10*, 064037.

(2) Wang, F.; Gao, F.; Lan, M.; Yuan, H.; Huang, Y.; Liu, J. Oxidative Stress Contributes to Silica Nanoparticle-Induced Cytotoxicity in Human Embryonic Kidney Cells. *Toxicol. In Vitro* **2009**, *23*, 808−815.

(3) Bakand, S.; Hayes, A.; Dechsakulthorn, F. Nanoparticles: A Review of Particle Toxicology Following Inhalation Exposure. *Inhalation Toxicol.* **2012**, *24*, 125−135.

(4) Lai, D. Y. Toward Toxicity Testing of Nanomaterials in the 21st Century: A Paradigm for Moving Forward. *Wiley Interdiscip. Rev.: Nanomed. Nanobiotechnol.* **2012**, *4*, 1−15.

(5) Ray, P. C.; Yu, H.; Fu, P. P. Toxicity and Environmental Risks of Nanomaterials: Challenges and Future Needs. *J. Environ. Sci. Health, Part C: Environ. Carcinog. Ecotoxicol. Rev.* **2009**, *27*, 1−35.

(6) Lewinski, N.; Colvin, V.; Drezek, R. Cytotoxicity of Nanoparticles. *Small* **2008**, *4*, 26−49.

(7) Love, S. A.; Maurer-Jones, M. A.; Thompson, J. W.; Lin, Y. S.; Haynes, C. L. Assessing Nanoparticle Toxicity. *Annu. Rev. Anal. Chem.* **2012**, *5*, 181−205.

(8) Sayes, C. M.; Reed, K. L.; Warheit, D. B. Assessing Toxicity of Fine and Nanoparticles: Comparing in Vitro Measurements to in Vivo Pulmonary Toxicity Profiles. *Toxicol. Sci.* **2007**, *97*, 163−180.

(9) Luyts, K.; Napierska, D.; Nemery, B.; Hoet, P. H. M. How Physico-Chemical Characteristics of Nanoparticles Cause Their Toxicity: Complex and Unresolved Interrelations. *Environ. Sci.: Processes Impacts* **2013**, *15*, 23−38.

(10) Xia, T.; Kovochich, M.; Liong, M.; Madler, L.; Gilbert, B.; Shi, H.; Yeh, J. I.; Zink, J. I.; Nel, A. E. Comparison of the Mechanism of Toxicity of Zinc Oxide and Cerium Oxide Nanoparticles Based on Dissolution and Oxidative Stress Properties. *ACS Nano* **2008**, *2*, 2121−2134.

(11) Oberdörster, G.; Maynard, A.; Donaldson, K.; Castranova, V.; Fitzpatrick, J.; Ausman, K.; Carter, J.; Karn, B.; Kreyling, W. G.; Lai, D. et al. Principles for Characterizing the Potential Human Health Effects from Exposure to Nanomaterials: Elements of a Screening Stragegy. *Part. Fibre Toxicol.* **2005**, *2*.

(12) Vandebriel, R. J.; De Jong, W. H. A Review of Mammalian Toxicity of Zno Nanoparticles. *Nanotechnol. Sci. Appl.* **2012**, *5*, 61−71.

(13) Castet, D.; Bouillard, J. Acute Pneumopathy Caused by Exposure to Zinc Oxide. *Rev. Mal. Respir.* **1992**, *9*, 632−633.

(14) Cho, W. S.; Duffin, R.; Poland, C. A.; Howie, S. E.; MacNee, W.; Bradley, M.; Megson, I. L.; Donaldson, K. Metal Oxide Nanoparticles Induce Unique Inflammatory Footprints in the Lung: Important Implications for Nanoparticle Testing. *Environ. Health Perspect.* **2010**, *118*, 1699−1706.

(15) Iavicoli, I.; Leso, V.; Bergamaschi, A. Toxicological Effects of Titanium Dioxide Nanoparticles: A Review of in Vivo Studies. *J. Nanomater.* **2012**, *2012*, 1−36.

(16) Jaganathan, H.; Godin, B. Biocompatibility Assessment of Si-Based Nano- and Micro-Particles. *Adv. Drug Delivery Rev.* **2012**, *64*, 1800−1819.

(17) Martin, C. J.; Le, X. C.; Guidotti, T. L.; Yalcin, S.; Chum, E.; Audette, R. J.; Liang, C.; Yuan, B.; Zhang, X.; Wu, J. Zinc Exposure in Chinese Foundry Workers. *Am. J. Ind. Med.* **1999**, *35*, 574−580.

(18) Srinivas, A.; Rao, P. J.; Selvam, G.; Murthy, P. B.; Reddy, P. N. Acute Inhalation Toxicity of Cerium Oxide Nanoparticles in Rats. *Toxicol. Lett.* **2011**, *205*, 105−115.

(19) Song, Y.; Li, X.; Wang, L.; Rojanasakul, Y.; Castranova, V.; Li, H.; Ma, J. Nanomaterials in Humans: Identification, Characteristics, and Potential Damage. *Toxicol. Pathol.* **2011**, *39*, 841−849.

(20) Hartung, T.; Sabbioni, E. Alternative in Vitro Assays in Nanomaterial Toxicology. *Wiley Interdiscip. Rev.: Nanomed. Nanobiotechnol.* **2011**, *3*, 545−573.

(21) Hillegass, J. M.; Shukla, A.; Lathrop, S. A.; MacPherson, M. B.; Fukagawa, N. K.; Mossman, B. T. Assessing Nanotoxicity in Cells in Vitro. *Wiley Interdiscip. Rev.: Nanomed. Nanobiotechnol.* **2010**, *2*, 219−231.

(22) Horie, M.; Kato, H.; Fujita, K.; Endoh, S.; Iwahashi, H. In Vitro Evaluation of Cellular Response Induced by Manufactured Nanoparticles. *Chem. Res. Toxicol.* **2012**, *25*, 605−619.

(23) Jones, C. F.; Grainger, D. W. In Vitro Assessments of Nanomaterial Toxicity. *Adv. Drug Delivery Rev.* **2009**, *61*, 438−456.
(24) Han, X.; Corson, N.; Wade-Mercer, P.; Gelein, R.; Jiang, J.; Sahu, M.; Biswas, P.; Finkelstein, J. N.; Elder, A.; Oberdorster, G. Assessing the Relevance of in Vitro Studies in Nanotoxicology by Examining Correlations Between in Vitro and in Vivo Data. *Toxicology* **2012**, *297*, 1−9.
(25) Nel, A.; Xia, T.; Meng, H.; Wang, X.; Lin, S.; Ji, Z.; Zhang, H. Nanomaterial Toxicity Testing in the 21st Century: Use of a Predictive Toxicological Approach and High-Throughput Screening. *Acc. Chem. Res.* **2013**, *46*, 607−621.
(26) Park, M. V.; Lankveld, D. P.; van Loveren, H.; de Jong, W. H. The Status of in Vitro Toxicity Studies in the Risk Assessment of Nanomaterials. *Nanomedicine* **2009**, *4*, 669−685.
(27) Holder, A. L.; Goth-Goldstein, R.; Lucas, D.; Koshland, C. P. Particle-Induced Artifacts in the Mtt and Ldh Viability Assays. *Chem. Res. Toxicol.* **2012**, *25*, 1885−1892.
(28) Kroll, A.; Pillukat, M. H.; Hahn, D.; Schnekenburger, J. Interference of Engineered Nanoparticles with in Vitro Toxicity Assays. *Arch. Toxicol.* **2012**, *86*, 1123−1136.
(29) Rushton, E. K.; Jiang, J.; Leonard, S. S.; Eberly, S.; Castranova, V.; Biswas, P.; Elder, A.; Han, X.; Gelein, R.; Finkelstein, J.; et al. Concept of Assessing Nanoparticle Hazards Considering Nanoparticle Dosemetric and Chemical/Biological Response Metrics. *J. Toxicol. Environ. Health, Part A* **2010**, *73*, 445−461.
(30) Muller, L.; Riediker, M.; Wick, P.; Mohr, M.; Gehr, P.; Rothen-Rutishauser, B. Oxidative Stress and Inflammation Response After Nanoparticle Exposure: Differences Between Human Lung Cell Monocultures and an Advanced Three-Dimensional Model of the Human Epithelial Airways. *J. R. Soc., Interface* **2010**, *7* (Suppl 1), S27−40.
(31) Huh, D.; Matthews, B. D.; Mammoto, A.; Montoya-Zavala, M.; Hsin, H. Y.; Ingber, D. E. Reconstituting Organ-Level Lung Functions on a Chip. *Science* **2010**, *328*, 1662−1668.
(32) Lulevich, V.; Shih, Y. P.; Lo, S. H.; Liu, G. Y. Cell Tracing Dyes Significantly Change Single Cell Mechanics. *J. Phys. Chem. B* **2009**, *113*, 6511−6519.
(33) Lulevich, V.; Yang, H. Y.; Isseroff, R. R.; Liu, G. Y. Single Cell Mechanics of Keratinocyte Cells. *Ultramicroscopy* **2010**, *110*, 1435−1442.
(34) Lulevich, V.; Zimmer, C. C.; Hong, H. S.; Jin, L. W.; Liu, G. Y. Single-Cell Mechanics Provides a Sensitive and Quantitative Means for Probing Amyloid-Beta Peptide and Neuronal Cell Interactions. *Proc. Natl. Acad. Sci. U. S. A.* **2010**, *107*, 13872−13877.
(35) Lulevich, V.; Zink, T.; Chen, H. Y.; Liu, F. T.; Liu, G. Y. Cell Mechanics Using Atomic Force Microscopy-Based Single-Cell Compression. *Langmuir* **2006**, *22*, 8151−8155.
(36) Zimmer, C. C.; Shi, L. F.; Shih, Y. P.; Li, J. R.; Jin, L. W.; Lo, S. H.; Liu, G. Y. F-Actin Reassembly During Focal Adhesion Impacts Single Cell Mechanics and Nanoscale Membrane Structure. *Sci. China Chem.* **2012**, *55*, 1922−1930.
(37) Gojova, A.; Guo, B.; Kota, R. S.; Rutledge, J. C.; Kennedy, I. M.; Barakat, A. I. Induction of Inflammation in Vascular Endothelial Cells by Metal Oxide Nanoparticles: Effect of Particle Composition. *Environ. Health Perspect.* **2007**, *115*, 403−409.
(38) Kreyling, W. G.; Semmler, M.; Erbe, F.; Mayer, P.; Takenaka, S.; Schulz, H.; Oberdorster, G.; Ziesenis, A. Translocation of Ultrafine Insoluble Iridium Particles from Lung Epithelium to Extrapulmonary Organs Is Size Dependent but Very Low. *J. Toxicol. Environ. Health, Part A* **2002**, *65*, 1513−1530.
(39) Nemmar, A.; Hoylaerts, M. F.; Hoet, P. H.; Vermylen, J.; Nemery, B. Size Effect of Intratracheally Instilled Particles on Pulmonary Inflammation and Vascular Thrombosis. *Toxicol. Appl. Pharmacol.* **2003**, *186*, 38−45.
(40) Ge, G.; Wu, H.; Xiong, F.; Zhang, Y.; Guo, Z.; Bian, Z.; Xu, J.; Gu, C.; Gu, N.; Chen, X.; et al. The Cytotoxicity Evaluation of Magnetic Iron Oxide Nanoparticles on Human Aortic Endothelial Cells. *Nanoscale Res. Lett.* **2013**, *8*, 215.
(41) Gojova, A.; Lee, J. T.; Jung, H. S.; Guo, B.; Barakat, A. I.; Kennedy, I. M. Effect of Cerium Oxide Nanoparticles on Inflammation in Vascular Endothelial Cells. *Inhalation Toxicol.* **2009**, *21* (Suppl 1), 123−130.
(42) Li, R.; Ning, Z.; Cui, J.; Khalsa, B.; Ai, L.; Takabe, W.; Beebe, T.; Majumdar, R.; Sioutas, C.; Hsiai, T. Ultrafine Particles from Diesel Engines Induce Vascular Oxidative Stress Via Jnk Activation. *Free Radical Biol. Med.* **2009**, *46*, 775−782.
(43) Li, R.; Ning, Z.; Cui, J.; Yu, F.; Sioutas, C.; Hsiai, T. Diesel Exhaust Particles Modulate Vascular Endothelial Cell Permeability: Implication of Zo-1 Expression. *Toxicol. Lett.* **2010**, *197*, 163−168.
(44) Moos, P. J.; Honeggar, M.; Malugin, A.; Herd, H.; Thiagarajan, G.; Ghandehari, H. Transcriptional Responses of Human Aortic Endothelial Cells to Nanoconstructs Used in Biomedical Applications. *Mol. Pharmacol.* **2013**, *10*, 3242−3252.
(45) Gilbert, B.; Fakra, S. C.; Xia, T.; Pokhrel, S.; Madler, L.; Nel, A. E. The Fate of Zno Nanoparticles Administered to Human Bronchial Epithelial Cells. *ACS Nano* **2012**, *6*, 4921−4930.
(46) Hanley, C.; Thurber, A.; Hanna, C.; Punnoose, A.; Zhang, J.; Wingett, D. G. The Influences of Cell Type and Zno Nanoparticle Size on Immune Cell Cytotoxicity and Cytokine Induction. *Nanoscale Res. Lett.* **2009**, *4*, 1409−1420.
(47) Kao, Y.-Y.; Chen, Y.-C.; Cheng, T.-J.; Chiung, Y.-M.; Liu, P.-S. Zinc Oxide Nanoparticles Interfere with Zinc Ion Homeostasis to Cause Cytotoxicity. *Toxicol. Sci.* **2012**, *125*, 462−472.
(48) Liu, X.; Sun, J. Endothelial Cells Dysfunction Induced by Silica Nanoparticles Through Oxidative Stress Via Jnk/P53 and Nf-Kappab Pathways. *Biomaterials* **2010**, *31*, 8198−8209.
(49) Ye, Y.; Liu, J.; Xu, J.; Sun, L.; Chen, M.; Lan, M. Nano-Sio2 Induces Apoptosis Via Activation of P53 and Bax Mediated by Oxidative Stress in Human Hepatic Cell Line. *Toxicol. In Vitro* **2010**, *24*, 751−758.
(50) Mohamed, B. M.; Verma, N. K.; Prina-Mello, A.; Williams, Y.; Davies, A. M.; Bakos, G.; Tormey, L.; Edwards, C.; Hanrahan, J.; Salvati, A.; et al. Activation of Stress-Related Signalling Pathway in Human Cells Upon Sio2 Nanoparticles Exposure as an Early Indicator of Cytotoxicity. *J. Nanobiotechnol.* **2011**, *9*, 29.
(51) Guo, B.; Kennedy, I. M. The Speciation and Morphology of Chromium Oxide Nanoparticles in a Diffusion Flame. *Aerosol Sci. Technol.* **2004**, *38*, 424−436.
(52) Cleveland, J. P.; Manne, S.; Bocek, D.; Hansma, P. K. A Nondestructive Method for Determining the Spring Constant of Cantilevers for Scanning Force Microscopy. *Rev. Sci. Instrum.* **1993**, *64*, 403−405.
(53) Sader, J. E.; Larson, I.; Mulvaney, P.; White, L. R. Method for the Calibration of Atomic-Force Microscope Cantilevers. *Rev. Sci. Instrum.* **1995**, *66*, 3789−3798.
(54) Sun, J.; Wang, S.; Zhao, D.; Hun, F. H.; Weng, L.; Liu, H. Cytotoxicity, Permeability, and Inflammation of Metal Oxide Nanoparticles in Human Cardiac Microvascular Endothelial Cells: Cytotoxicity, Permeability, and Inflammation of Metal Oxide Nanoparticles. *Cell Biol. Toxicol.* **2011**, *27*, 333−342.
(55) Sharma, V.; Anderson, D.; Dhawan, A. Zinc Oxide Nanoparticles Induce Oxidative DNA Damage and Ros-Triggered Mitochondria Mediated Apoptosis in Human Liver Cells (Hepg2). *Apoptosis* **2012**, *17*, 852−870.
(56) Barbee, K. A.; Davies, P. F.; Lal, R. Shear Stress-Induced Reorganization of the Surface Topography of Living Endothelial Cells Imaged by Atomic Force Microscopy. *Circ. Res.* **1994**, *74*, 163−171.
(57) Donnini, D.; Perrella, G.; Stel, G.; Ambesi-Impiombato, F. S.; Curcio, F. A New Model of Human Aortic Endothelial Cells in Vitro. *Biochimie* **2000**, *82*, 1107−1114.
(58) Birukova, A. A.; Arce, F. T.; Moldobaeva, N.; Dudek, S. M.; Garcia, J. G.; Lal, R.; Birukov, K. G. Endothelial Permeability Is Controlled by Spatially Defined Cytoskeletal Mechanics: Atomic Force Microscopy Force Mapping of Pulmonary Endothelial Monolayer. *Nanomedicine* **2009**, *5*, 30−41.

(59) Costa, K. D.; Sim, A. J.; Yin, F. C. Non-Hertzian Approach to Analyzing Mechanical Properties of Endothelial Cells Probed by Atomic Force Microscopy. *J. Biomech. Eng.* **2006**, *128*, 176−184.
(60) Dahl, K. N.; Engler, A. J.; Pajerowski, J. D.; Discher, D. E. Power-Law Rheology of Isolated Nuclei with Deformation Mapping of Nuclear Substructures. *Biophys. J.* **2005**, *89*, 2855−2864.
(61) Li, C. H.; Liao, P. L.; Shyu, M. K.; Liu, C. W.; Kao, C. C.; Huang, S. H.; Cheng, Y. W.; Kang, J. J. Zinc Oxide Nanoparticles-Induced Intercellular Adhesion Molecule 1 Expression Requires Rac1/Cdc42, Mixed Lineage Kinase 3, and C-Jun N-Terminal Kinase Activation in Endothelial Cells. *Toxicol. Sci.* **2012**, *126*, 162−172.
(62) Lin, W. S.; Xu, Y.; Huang, C. C.; Ma, Y. F.; Shannon, K. B.; Chen, D. R.; Huang, Y. W. Toxicity of Nano- and Micro-Sized Zno Particles in Human Lung Epithelial Cells. *J. Nanopart. Res.* **2009**, *11*, 25−39.
(63) Deng, X.; Luan, Q.; Chen, W.; Wang, Y.; Wu, M.; Zhang, H.; Jiao, Z. Nanosized Zinc Oxide Particles Induce Neural Stem Cell Apoptosis. *Nanotechnology* **2009**, *20*, 115101.
(64) Deng, Z.; Lulevich, V.; Liu, F. T.; Liu, G. Y. Applications of Atomic Force Microscopy in Biophysical Chemistry of Cells. *J. Phys. Chem. B* **2010**, *114*, 5971−5982.